Journal of Ceramic Processing Research. Vol. 19, No. 4, pp. 285~289 (2018)

J O U R N A L O F
Ceramic Processing Research

Fabrication of a symmetrical microtubular SOFC single cell with catalyst-impregnated YSZ scaffold using an electrophoretic deposition process

Sang-Hoon Lee[a] and Ki-Tae Lee[a,b,*]

[a]*Division of Advanced Materials Engineering, Chonbuk National University Jeonbuk 54896 Korea*
[b]*Hydrogen and Fuel Cell Research Center, Chonbuk National University, Jeonbuk 54896 Korea*

Symmetrical microtubular solid oxide fuel cells (SOFCs) with a catalyst-impregnated yttria-stabilized zirconia (YSZ) scaffold were fabricated via electrophoretic deposition (EPD). While the pH of the prepared slurry decreased with the amount of phosphate ester (PE) as a charging agent, the electrical conductivity increased. Both the YSZ scaffold and electrolyte slurries with 0.5 wt% PE were stable over 36 h. The deposit thickness of the YSZ electrolyte layer increased with the applied voltage and deposition time. Due to the symmetrical scaffold structure, a single cell could be obtained by a one-step co-firing process. Fine Ni and $La_{0.6}Sr_{0.4}CoO_{3-\delta}$ (LSC) catalysts for anodes and cathodes, respectively, can be impregnated and distributed uniformly into the porous YSZ scaffold by a glycine-mediated impregnation technique. The maximum power density was 59, 67, and 71 mW/cm^2 at 600, 700, and 800 °C, respectively. After the 50th redox cycle, the single cell exhibited no significant performance degradation.

Key words: Solid oxide fuel cells, Symmetrical micro tubular single cell, Electrophoretic deposition, Scaffold, Impregnation, Redox stability.

Introduction

Solid oxide fuel cells (SOFCs) have many advantages because SOFCs can be operated at high temperature (500-1000 °C). A high temperature makes it possible to use an inexpensive catalyst and have a high conversion efficiency because of high reaction kinetics, and the SOFC can also be combined with other heat generation systems [1-4]. Additionally, various gases such as CO, CH_4, and syngas can be use as fuels [5].

SOFCs can be roughly classified by planar and tubular types. Even though planar SOFCs have high performance and efficiency, they need sealant to block the gas leakage [6-10]. However, the tubular SOFCs do not need to seal. Meanwhile, miniaturization of tubular SOFCs can maximize these advantages, because the micro size provides stability during the cooling and heating cycles [11-13], which is very important to a quick operating process. Additionally, the microtubular SOFCs are suitable for stacking single cells. Although a high operating temperature has many benefits, critical weaknesses also exist for durability such as thermal expansion, reactions between single cell components, and instability in a redox atmosphere. Among these problems, redox stability has been significantly studied by current research [14, 15].

*Corresponding author:
Tel : +82-63-270-2290
Fax: +82-63-270-2386
E-mail: ktlee71@jbnu.ac.kr

The scaffold has a porous skeletal structure. The electrolyte can extend to the electrode region in the form of a backbone, so that the strength of the whole single cell is greatly improved. Moreover, scaffold anodes of yttria-stabilized zirconia (YSZ) or other oxides, such as a $La_{0.7}Ca_{0.3}Cr_{0.8}Mn_{0.2}O_{3-\delta}$ (LCCM), are less affected by the redox reaction than Ni-based anodes. In particular, the symmetrical scaffold structure has a relatively simple manufacturing process (molding → sintering → catalyst impregnation → heat treatment) compared to the conventional process (anode support extrusion → anode pre-sintering → electrolyte coating → anode/electrolyte sintering → cathode coating → cathode sintering), which results in a significant reduction in manufacturing cost. Since the heat treatment for preparation of the catalyst layer is performed at a relatively low temperature (600 °C or less), the growth of the catalyst, such as Ni, can be suppressed compared to the conventional method. Therefore, the interfacial reaction between the electrolyte and electrode, which may occur during the high temperature heat treatment process, can be minimized.

The electrophoretic deposition (EPD) process was used by Harsanyi in 1927 [16]. This technology is similar to the plating of a thin layer of metal on some surface or covering of metal plates. EPD can deposit uncharged materials such as ceramics, polymers, and metals [17]. A charging agent helps enclose the surface of the colloidal particles to be influenced by the electric field [18]. Thus, EPD can freely control the degree of deposition by applied voltage and deposition time.

Therefore, it is very simple and fast to fabricate complex layers [19, 20]. Alternatively, to make an EPD slurry, a suitable solvent is needed to dissolve the dispersant [21]. In addition, when the solvent evaporates, it should not cause cracks or pores. Because of this, organic solvents are widely used. Lastly, a slurry is prepared by adding a binder to prevent cracking [22].

In this study, symmetrical microtubular SOFC single cells with a catalyst-impregnated YSZ scaffold were fabricated via EPD, and their property and electrochemical performance were investigated.

Experimental Procedure

The most important condition in EPD is to prepare a stable slurry. The YSZ scaffold slurry consisted of YSZ (TZ-8YS, Tosoh, Japan), PMMA (SUNPMMA-S100, Sunjin Chemical, Korea) as a pore former, polyvinyl butyral (PVB, Sigma-Aldrich, Germany) as a binder, phosphate ester (PE, ethyl acid phosphate, Johoku Chemical, Japan) as a dispersant, and anhydrous ethanol as an organic solvent. The YSZ electrolyte slurry was similarly prepared without PMMA. All components of each slurry were thoroughly mixed by ball-milling for 15 h.

The prepared stable slurries for the YSZ scaffold anode layer, YSZ electrolyte layer, and YSZ scaffold cathode layer were deposited sequentially on a graphite rod (3-mm diameter, Alfa Aesar, England). The deposition conditions were controlled by various voltages and times at a constant current of 20 mA. The as-deposited green bodies were sintered at 1400 ºC for 5 h in air.

The next step is impregnation of the catalyst, such as Ni and $La_{0.6}Sr_{0.4}CoO_{3-\delta}$ (LSC), into the porous YSZ anode and cathode scaffold, respectively. A glycine-mediated impregnation technique was used as previously reported [23]. The precursor material for the Ni catalyst was $Ni(NO_3)_2{\cdot}6H_2O$ (Puratronic®, 99.9985% metals basis, Alfa Aesar, England). A 0.01 M Ni stock solution was prepared with glycine (99%, Alfa Aesar, England). For the LSC, $La(NO_3)_3{\cdot}5H_2O$ (99.9% metal basis, Sigma-Aldrich, Germany), $Sr(NO_3)_2$ (99.0%, Alfa Aesar, England), and $Co(NO_3)_2{\cdot}6H_2O$ (Puratronic®, 99.999%, metals basis, Alfa Aesar, England) were used as the precursor materials with glycine (99%, Alfa Aesar, England). Impregnation was carried out by micro pipetting three times. Subsequently, the impregnated samples were kept inside a vacuum oven for 1 h at 80 ºC. This was followed by calcination at 800 ºC for Ni catalyst and 950 ºC for LSC catalyst for 2 h in air.

Au paste as a current collector was deposited on both the cathode and anode sides and then fired at 800 ºC for 1 h. A galvano-potentiostat (SP150, Biologic, SAS, France) was used for evaluating the electrochemical performance at 600-800 ºC. Humidified H_2 (~3% H_2O at 30 ºC) and dry air were supplied as a fuel and oxidant at flow rates of 30 and 100 cm^3/min, respectively. For the redox cycle test, a single cell operated at a constant current load of 70 mA/cm^2 at 600 ºC with H_2 fuel for 30 min and air for 30 min. N_2 gas was purged for 30 min between H_2 and air flow.

Results and Discussion

The first step of the EPD process is to prepare a stable slurry for each coating layer. The YSZ scaffold slurry and YSZ electrolyte slurry were prepared. Although the two slurries are based on the same YSZ powder, their compositions should be different because the electrolyte and scaffold must have different microstructures. The particles in the slurry should be well dispersed to be stable and charged to be moved by the electrical field. PE was used as a dispersant as well as a charging agent in this study. The hydroxyl group in the organic solvent combines with the dissociated PE molecules with negatively charged O sites and releases the proton. The released protons are absorbed on the surface of the particle in the slurry as a result of the interaction between the acid and base [24]. Therefore, the particles are charged positively. The pH and electrical conductivity of the YSZ scaffold and YSZ electrolyte slurries measured with various amounts of PE are shown in Fig. 1. When the amount of PE increases, the pH decreases, but the electrical

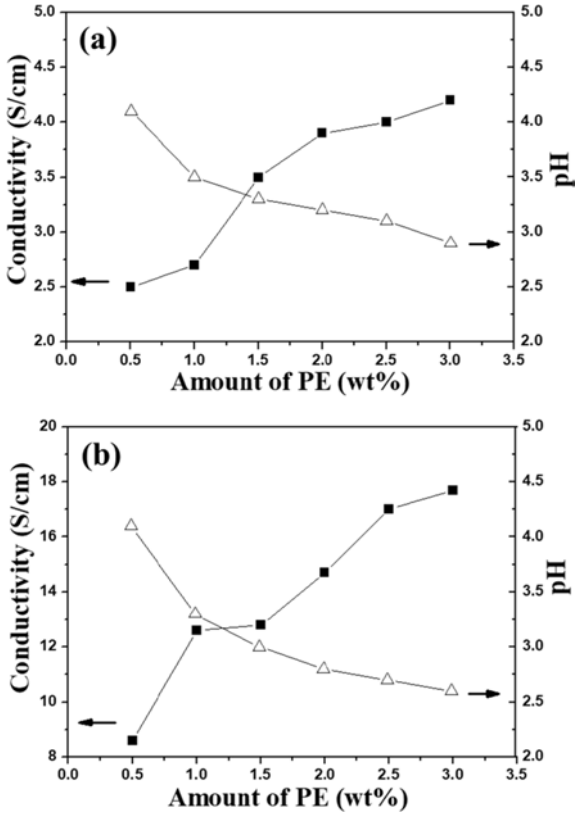

Fig. 1. Conductivity and pH of the YSZ (a) scaffold and (b) electrolyte slurries as a function of PE concentration.

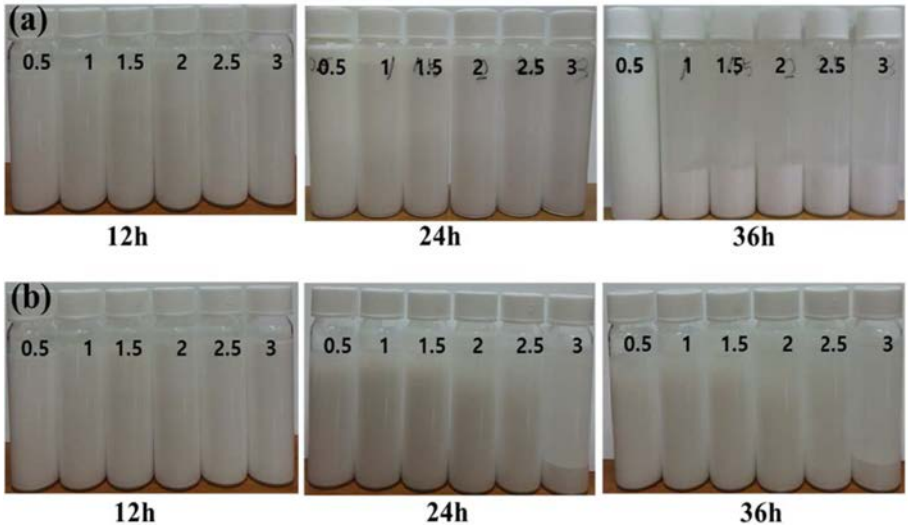

Fig. 2. Stability of the YSZ (a) scaffold and (b) electrolyte slurry with time. The numbers in the picture indicate the amount of PE.

Table 1. Optimal slurry conditions for the EPD process.

Slurry	PE (wt%)	PVB (wt%)	PMMA (vol%)	Solid loading (solute: solvent)
YSZ scaffold	0.5	2.5	30	28:100
YSZ electrolyte	0.5	2.5	–	20:100

conductivity increases due to an increase in the amount of released protons.

Alternatively, the separated PE molecules coordinate with protonated positive sites on the surfaces of particles and consequently prevent flocculation as a dispersant. The dispersion stability of each slurry with various amounts of PE was evaluated by a precipitation test as shown in Fig. 2. The YSZ scaffold slurry exhibited no layer separation until 24 h, but the samples that contained more than 1 wt% PE showed precipitation after 36 h. The super-saturation of PE on the surface of particles may induce precipitation. In the case of the YSZ scaffold slurry, only the sample containing 0.5 wt% PE was stable over 24 h. Accordingly, the optimal amount of PE for the preparation of both a stable YSZ scaffold and YSZ electrolyte slurries was confirmed as 0.5 wt%. The optimal conditions for the slurry of the YSZ scaffold and YSZ electrolyte layers are listed in Table 1.

In order to investigate the deposition rate according to EPD conditions, the thickness and weight of the deposited green body samples dried for 24 h at room temperature were measured while varying the voltage and deposition time, respectively, at the fixed current of 20 mA; the results are shown in Fig. 3. While both the deposition weight and thickness of the YSZ electrolyte increased linearly with increasing deposition time at the fixed current and voltage, both increased up to 15 V and were saturated at 30 V. Based on these results, the

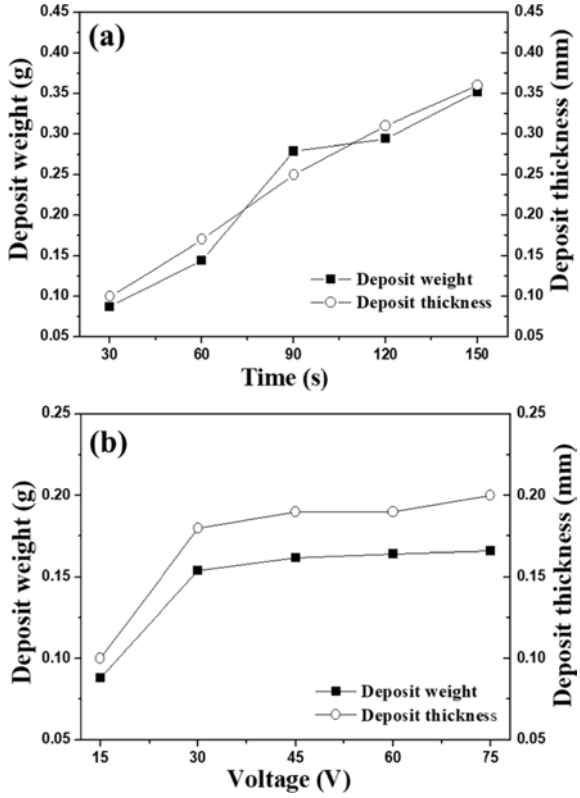

Fig. 3. The deposition weight and thickness of the YSZ electrolyte as a function of the (a) deposition time at 10 V and (b) voltage for 20 s.

optimal deposition conditions for each coating layer in order to obtain crack-free rigid samples are listed in Table 2.

Fig. 4 shows a cross-sectional SEM image and an image of the symmetrical microtubular SOFC single cells with YSZ scaffold that was fabricated by the EPD process with a 2.5 mm diameter and 60 mm length after sintering at 1400 ºC for 5 h in air. No delamination or

Table 2. Optimal deposition conditions for the EPD process.

Layer	Voltage (V)	Current (mA)	Time (s)
YSZ scaffold anode	20	20	60
YSZ electrolyte	10	20	10
YSZ scaffold cathode	8	20	8

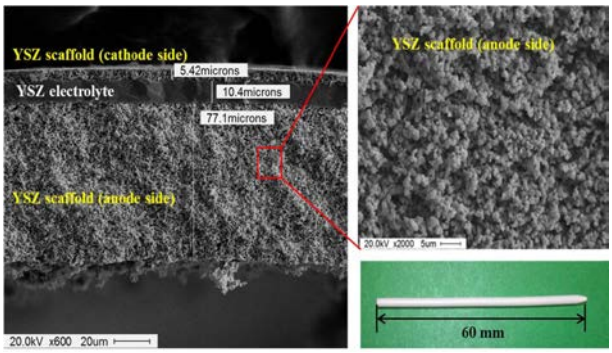

Fig. 4. Cross-sectional SEM image and picture of the symmetrical microtubular SOFC single cells with YSZ scaffold that was fabricated by the EPD process.

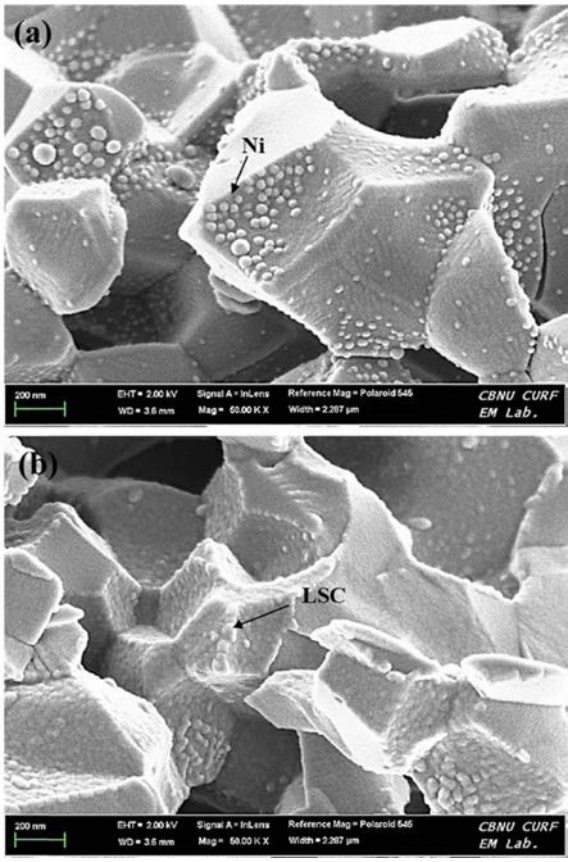

Fig. 5. Cross-sectional SEM images of Ni and LSC particles located in the YSZ scaffold structure of the (a) anode and (b) cathode side, respectively.

cracks were observed between the porous scaffold and dense electrolyte layers. A thin YSZ electrolyte with 10.4 μm thickness was deposited evenly. The effective electrode area was 4.7 cm^2.

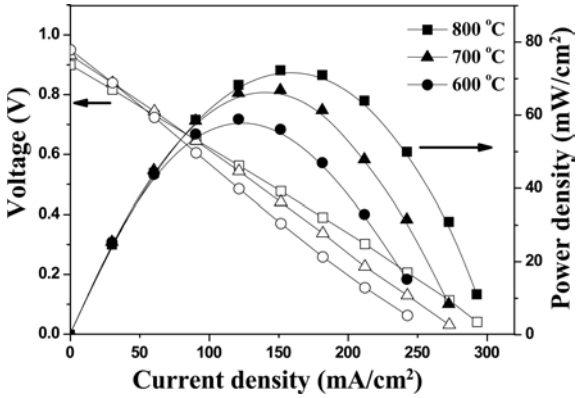

Fig. 6. Current-voltage (I-V) and power density curves for the symmetrical microtubular SOFC single cells with catalyst-impregnated YSZ scaffold fabricated by the EPD process, measured at 600-800 °C.

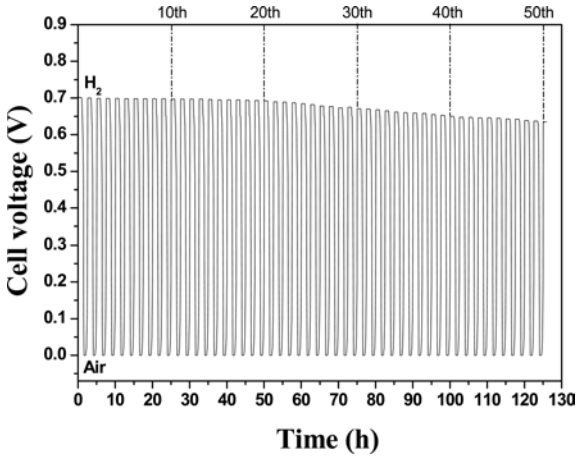

Fig. 7. Redox stability of the symmetrical microtubular SOFC single cells with catalyst-impregnated YSZ scaffold fabricated by the EPD process, measured at 600 °C.

Ni and LSC catalysts were impregnated into the porous YSZ anode and cathode scaffold, respectively. In the case of Ni catalyst, NiO was the as-impregnated form after calcination in air. In reality, NiO would be reduced to Ni during the operation. The microstructures of the catalyst-impregnated cathode and anode are shown in Fig. 5. NiO was reduced to Ni at 800 °C for 2 h in H_2. Fine Ni and LSC particles were homogeneously distributed onto the YSZ scaffold. However, Ni particles were distributed discontinuously, while the LSC particles evenly covered the YSZ surface.

Current-voltage (I-V) and power density curves for the symmetrical microtubular SOFC single cells with catalyst-impregnated YSZ scaffold fabricated by the EPD process, measured at 600-800 °C, are shown in Fig. 6. The open circuit voltage values at 600, 700, and 800 °C were 0.95, 0.93, and 0.90 V, respectively, which are less than the theoretical value for the YSZ electrolyte-based single cell. This indicates that gas leakage might occur through the pin-holes on the thin YSZ electrolyte. The maximum power density was 59, 67, and 71 mW/cm^2 at 600, 700, and 600 °C, respectively.

Although the single cell exhibited relatively lower electrochemical performance compared to the conventional YSZ electrolyte-based single cells, it showed no significant performance degradation and a 91% high performance retention rate after 50 redox cycles, as shown in Fig. 7.

Conclusions

Symmetrical microtubular SOFC single cells with YSZ scaffold were fabricated successfully via EPD. The stability of the slurry is strongly affected by the amount of charging agent such as PE. The thickness and morphology of the dense or porous layers can be precisely controlled by manipulating the deposition time and voltage. Uniformly-distributed fine Ni and LSC particles as catalysts for the anode and cathode, respectively, were successfully impregnated into the porous YSZ scaffold by a glycine-mediated impregnation technique. Unlike conventional SOFC single cells, symmetrical microtubular SOFC single cells with YSZ scaffold fabricated using the EPD process can be obtained by a one-step co-firing process. Although the symmetrical microtubular SOFC single cell with catalyst-impregnated YSZ scaffold fabricated by EPD exhibited relatively low electrochemical performance at intermediate temperatures, it showed significant redox stability.

Acknowledgements

This work was supported by the Technology Development Program to Solve Climate Changes of the National Research Foundation (NRF) grant funded by the Korea government (Ministry of Science and ICT) (2017M1A2A2044930). This work was also supported by the Korea Institute of Energy Technology Evaluation and Planning (KETEP) and the Ministry of Trade, Industry & Energy (MOTIE) of the Republic of Korea (No. 20164030201070).

References

1. K. Eguchi, Y. Kunisa, K. Adachi, H. Arai, J. Electrochem. Soc. 143 (1996) 3699.
2. H. Djamel, A. Hafsia, Z. Bariza, Ben M. Hocine, O. Kafia, Int. J. Hydrogen Energy 38 (2013) 8575.
3. J. Kibsgaard, C. Tsai, K. Chan, J.D. Benck, J.K. Nørskov, F. Abild-Pedersen, T.F. Jaramillo, Energy Environ. Sci. 8 (2015) 3022.
4. W. Sheng, A.P. Bivens, M. Myint, Z. Zhuang, R.V. Forest, Q. Fang, J.G. Chen, Y. Yan, Energy Environ. Sci. 7 (2014) 1719.
5. T. S. Doyle, Z. Dehouche, P.V. Aravind, M. Liu, S. Stankovic, Int. J. Hydrogen Energy 39 (2014) 12083.
6. C. Chen, M. Liu, L. Yang, M. Liu, Int. J. Hydrogen Energy 36 (2011) 5604.
7. J.S. Cherng, N.Y. Ho, T.H. Yeh, W.H. Chen, Ceram. Int. 38 (2012) S477.
8. X. Vien Nguyen, C. Tsair Chang, G. Bin Jung, S. Hung Chan, W. Tai Lee, S. Wei Chang, I. Kao, Int. J. Hydrogen Energy 41 (2016) 21812.
9. H. Kim, W.J. Kim, J.W. Lee, S.B. Lee, T.H. Lim, S.J. Park, R.H. Song, D.R. Shin, Korean J. Chem. Eng. 50 [4] (2012) 749.
10. J.S. Cherng, C.C Wu, F.A. Yu, T.H. Yeh, J. Power Sources 232 (2013) 353.
11. M. Torrell, A. Morata, P. Kayser, M. Kendall, K. Kendall, A. Tarancón, J. Power Sources 285 (2015) 439.
12. T. Matsui, J. Kim, H. Muroyama, M. Shimazu, T. Abe, M. Miyao, K. Eguchi, Solid State Ionics 225 (2012) 50.
13. C. Yang, C. Jin, M. Liu, F. Chen, Electrochem. Commun. 34 (2013) 231.
14. M. Boaro, A. Pappacena, C. Abate, M. Ferluga, J. Llorca, A. Trovarelli, J. Power Sources 270 (2014) 79.
15. L. Fan, Y. Xiong, Y. Wang, H. Kishimoto, K. Yamaji, T. Horita, J. Power Sources 294 (2015) 452.
16. J. Li, Y.J. Wu, T. Yamamoto, M. Kuwabara, Sci. Technol. Adv. Mater. 5 (2004) 393.
17. J.J.V. Tassel, C.A. Randall, Key Eng. Mater. 314 (2006) 167.
18. Y. Fukada, N. Nagarajan, W. Mekky, Y. Bao, H.S. Kim, J. Mater. Sci. 39 (2004) 787.
19. K. Yamaji, H. Kishimoto, Y. Xiong, T. Horita, N. Sakai, H. Yokokawa, Solid State Ionics 175 (2004) 165.
20. P. Sarkar, J. Mater. Sci. 39 (2004) 819.
21. L. Besra, S. Zha, M. Liu, J. Power Sources 160 (2006) 207.
22. C. Nicollet, A. Flura, V. Vibhu, A. Rougier, J. Bassat, J. Grenier, Int. J. Hydrogen Energy 41 (2016) 15538.
23. M.K. Rath, K.T. Lee, Electrochim. Acta 212 (2016) 678.
24. S. Doungdaw, T. Uchikoshi, Y. Noguchi, C. Eamchotchawalit, Y. Sakka, Sci. Tech. Adv. Mater. 6 (2005) 927.